

# **Architecture and sequence stratigraphy of the Upper Coralline Limestone formation, Malta – implications for Eastern Mediterranean restriction prior to the Messinian Salinity Crisis**

Bialik, Or M.<sup>1\*</sup>; Zammit, Ray<sup>1,2</sup>; Micallef, Aaron<sup>1,3</sup>

1. Marine Geology & Seafloor Surveying, Department of Geosciences, University of Malta, Msida, MSD 2080, Malta.

2. School of Earth and Environmental Sciences, Cardiff University, Main Building, Park Place, Cardiff, CF10 3AT, United Kingdom.

3. GEOMAR Helmholtz Centre for Ocean Research Kiel, Wischhofstraße 1-3, 24148 Kiel, Germany.

\*Corresponding author ([or.bialik@um.edu.mt](mailto:or.bialik@um.edu.mt))

## **Abstract**

The Eastern and Western Mediterranean are separated by an elevated plateau that regulates water exchange between these two basins. The Maltese archipelago, situated atop this topographic high, offers a unique window into the evolution of this plateau in the lead up to the Messinian Salinity Crisis (MSC). The Upper Coralline Limestone formation was deposited between the late Tortonian and the early Messinian and was likely terminated by paleoceanographic events related to the MSC. It represents the youngest Miocene sedimentary deposits outcropping in the Maltese archipelago. This shallow-water carbonate unit can be used to trace paleoenvironmental changes atop the sill between the Eastern and Western Mediterranean and to explain the possible water flow restrictions to the Eastern Mediterranean that could have preceded the MSC. Here we combine field surveys and analysis of the depositional environment within the Upper Coralline Limestone in Malta, with recently acquired multichannel seismic reflection profiles between Malta and Gozo, to reconstruct the depositional sequence in the Malta Plateau during the late Miocene.

The Upper Coralline Limestone consists of multiple coralline and larger benthic foraminifera dominated facies, extending from subtidal to intertidal environments. These accumulated in two depositional cycles observed in both outcrop and seismic reflection data. Each cycle exhibits an early aggradation-progradation phase followed by progradation phase and a final aggradation phase. These manifest themselves in the outcrops as shallowing and deepening upwards phases. These were deposited above a deep water unit and indicated a preceding uplift phase followed by filling of the accommodation space through the deposition of the Upper Coralline Limestone formation in shallow marine depths. These indicate the presence of a highly elevated sill during the late Miocene, which could have restricted circulation to the eastern basin.

**Keywords:** Carbonate platform, Malta Plateau, late Miocene C type carbonate factory, Central Mediterranean

## Introduction

The Messinian Salinity Crisis (MSC, 5.97 Ma to 5.33 Ma) was the result of extreme restriction of the Mediterranean Sea from the Atlantic Ocean (Hsü et al., 1973; Meilijson et al., 2019; Roveri et al., 2014a). Yet the impact and effect of the MSC were not uniformly distributed. The Eastern Mediterranean hosts around 70% of total MSC salt deposits, in significantly thicker deposits than the Western Mediterranean (Haq et al., 2020), indicating a marked difference in hydrology during the MSC. While it is accepted that evaporite deposition was synchronous in both the Western and Eastern Mediterranean (Krijgsman et al., 2002; Meilijson et al., 2019, 2018), an ongoing debate persists on whether the Eastern and Western Mediterranean were restricted to the same degree and at the same times (Blanc, 2000, 2006; Meijer, 2006; Ryan, 2008). In the aftermath of the MSC (the Zanclean flood), the western basin was the first to be reflooded. Subsequent flooding of the Eastern Basin occurred via a massive waterfall over the Maltese Escarpment due to overflow from the Western Basin (Garcia-Castellanos et al., 2020; Spatola et al., 2020).

$^{87}\text{Sr}/^{86}\text{Sr}$  isotope ratio analysis of carbonate deposits in the Eastern Mediterranean exhibit a departure from oceanic values, indicating modification and possible restriction from the world's oceans already during the late Tortonian (Schildgen et al., 2014). Reef accumulation patterns in the Eastern Mediterranean diverge from that of the Western Mediterranean, both in respect to number and composition (Buchbinder, 1996). Microfossil assemblages exhibit indications of periodically enhanced salinity and oxygen limitation (Kontakiotis et al., 2019; Kouwenhoven et al., 2006; Moissette et al., 2018). All of this evidence points to some enhanced restriction of the eastern basin as early as ~7.5 Ma.

A key region controlling the connection between the Eastern and Western Mediterranean is the sill between Sicily in the north and Tunisia in the south. This sill is part of the North African continental margin (Jongsma et al., 1985). This is a tectonically complex region where rifting, transpression and the African/European collision resulted in a highly dynamic configuration throughout the Miocene (Ben-Avraham et al., 1987; Dart et al., 1993; Gardiner et al., 1995). This allowed for significant vertical movements, well expressed in the geological record of the Maltese Islands by significant shifts in depositional depth (Pedley, 1978). In this study, we focus on the sedimentary evolution of this area and, mainly, on the depositional sequence of the late Tortonian and Messinian ages, prior to the MSC. This study aims to delineate the evolution of the sequence during this time. By integrating outcrop and seismic reflection data, we set to explore possible indications of vertical fill that could have resulted in the restriction of water exchange between the Eastern and Western Mediterranean.

## Geological setting

The Maltese archipelago is a relic of an ancient carbonate platform located in the northeastern part of the Pelagian block and dating back at least to the Paleogene (Gatt and Gluyas, 2012; Micallef et al., 2016). This greater structure dates back to the early stages of the Tethys Ocean and has since been relatively higher than its surroundings (Jongsma et al., 1985). During the late Miocene, this area experienced further uplift driven by SE-NW directed horizontal shortening as plate convergence between Africa and Europe changed the regional tectonic stress field (Adam et al., 2000; Gutscher et al., 2016; Reuther et al., 1993). These large magnitude vertical shifts of the Malta Plateau are well illustrated in the late Miocene by the transition from the hemipelagic Serravallian Blue Clay Formation to the shallow-water carbonates of the Tortonian-Messinian Upper Coralline Limestone (UCL) Formation, which are separated by a glauconitic unit referred to as the Greensand Formation (Baldassini and Di Stefano, 2017; Catanzariti and Gatt, 2014).

The UCL is a calcareous shallow marine succession and the youngest Miocene rock unit exposed in the Maltese Archipelago (Pedley, 1978). The age of the base of the UCL had been recently assigned to the upper part of Nannofossil zone MNN11a (CNM16, ~8 Ma; Baldassini and Di Stefano, 2017), while the age of its uppermost part is unknown and inferred to be either shortly after the Messinian Salinity Crisis (Pedley, 2011) or within the early part of the MSC (Cornée et al., 2004). Early interpretation, based on sedimentary components and modern coralline algae, described the deposition of the UCL as a shallowing upward sequence (Pedley, 1978; Table 1). It does not exhibit any of the extreme stress features reported in the Calcare di Base (Borrelli et al., 2020), and thus probably represent more moderate conditions. The geometry of the unit was inferred to be a belt of coralline bioherms (Bosence and Pedley, 1982; Pedley, 1976) aligned southeast-northwest along the southern margin of the island, developed atop a paleorelief. The individual beds described are representative of different lateral and temporal positions with respect to a carbonate platform (Cornée et al., 2004). Nevertheless, the described elements delineate the depositional depth of the UCL to <100 m in the deeper parts, and intertidal depths in the shallowest parts.

## Methods

### Field data

Fieldwork in 2017 included a systemic survey of UCL outcrops on the western side of the island of Malta. Five outcrops were chosen for study (from north to south, Figure 1): Anchor Bay (35.93°N/14.34°E; 13m), Rđum Majjiesa (35.94°N/14.33°E; 18m), Ġħajn Tuffieħa (35.93°N/14.34°E; 8.5m), Santi (35.82°N/14.36°E; 16m) and Bobbyland (35.85°N/14.37°E; 4m). Additionally, outcrops at St. Paul’s Bay; Rđum il-Qammieħ; Ras il-Pellegrin; Mellieħa; the range between Blata tal-Melħ and Rđum tal-Vigarju; Rđum il-Ħmar and the Bingemma syncline (white markers in Figure 1) were visited to examine the appearance and larger scale geometries. Field description of the unit was done using the modified Dunham (1962) classification by Embry and Klován (1971). These outcrops were selected to represent a near-complete representation of UCL depositional sequence in Malta; they contain within them most of the known facies of the UCL in the island of Malta except for the “Qammieħ beds” facies (Pedley, 1978), which does not outcrop in any of the surveyed sites. Some 96 samples were collected and analyzed using XRD Rigaku MiniFlex 600 benchtop X-ray diffractometer (30 kV/10 mA from 3° to 70° at 0.05° increments by point detector) to test viability for geochemical analysis. However, all samples exhibit full recrystallization to low Mg calcite and were excluded from further analysis since it has been assumed that any geochemical signal represents diagenetic conditions.

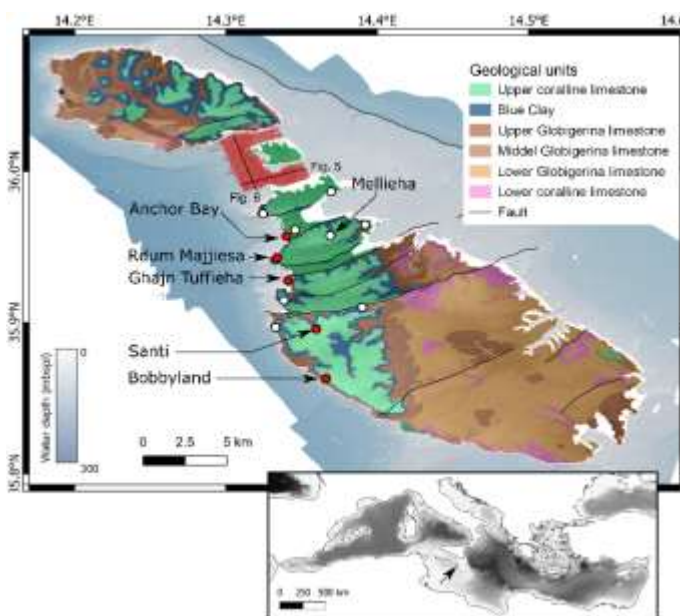


**Figure 1:** geological map of the Maltese archipelago showing the location of the study sites and area covered by the seismic survey. Location of columnar sections showed in Figure 2 are noted in red with names. Arrow in inset map shows the location of the Maltese archipelago in the modern Mediterranean.

## Geophysical data

Seismic interpretation was carried out on 240 km of multichannel seismic reflection profiles from the Gozo Channel project (Figure 1, more detailed image shown in Figure S1) using a mini GI gun with a total volume of 60 cu. in. (1 l). A shot point distance of 15.625–18.750 m and a recording length of 2 s were used. Data were recorded using a 300 m long digital streamer with 96 channels, with a channel distance of 3.125 m. The fold coverage ranged between 8 and 9.6 traces per CDP. The processing sequence included amplitude recovery, bandpass filtering, CDP sorting, pre-stack deconvolution, velocity analyses, normal move out correction, and stacking.

Based on existing knowledge (Pedley, 1976), we have limited our investigation to the upper 200 ms (milliseconds) of the seismic data. The sequence has been subdivided into seismic units (SUs) based on unconformities and seismic facies. These SU were numbered from bottom to top.

Member	Bed	Facies	Thickness (m)	Water depth	Environment
Gebel Imbarkk	Qammieh		25	Intertidal to very shallow subtidal (0-~5m)	Restricted intertidal to shallow marine (coastal lagoon?)
	Tat Tomna		2.3	Intertidal (0-1m)	Open intertidal to shallow marine
Tal Pitkal	Depiru	Ghadira	>23	Intertidal to very shallow subtidal (0-~5m)	Open intertidal to shallow marine
		Ghar Lapsi	25	Intertidal to very shallow subtidal (0-~5m)	Intertidal to shallow marine, pos. restricted
		<i>Sensu stricto</i>	3	<25m	Open marine shallow waters *1m marl layers are present
	Rabat Plateau		?	12-15m	Open marine shallow waters
Mtarfa	Rdum il-Hmar		12	<100m	Mid shelf open marine
	Gebel Mtarfa	<i>Sensu stricto</i>	7		Mid shelf open marine
		Coralline Algal bioherm	16	15-25m	Inner shelf open marine
Ghajn Melel	Zebbug		16.5	<50m	Mid shelf open marine
	Ghajn Znuber		5.1	Sublittoral (<200m)	Mid to outer shelf open marine, Pos. at interaction with OMZ

**Table 1:** Original subdivision of the UCL (Pedley, 1978) to members and beds, their assigned depositional settings and water depth.

## Results

### Outcrops

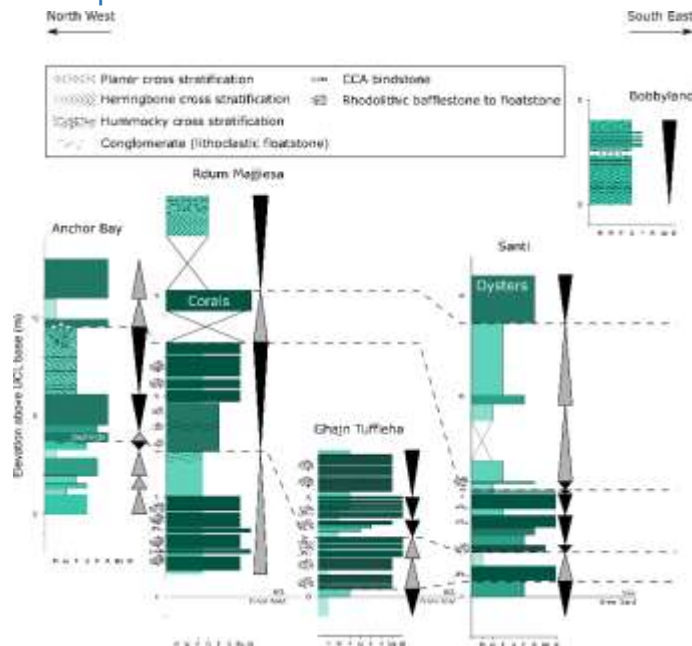


**Figure 2:** columnar sections of the investigated outcrops showing the present facies and features in each locality.

rhodoliths were observed in Santi and Ghajn Tuffieħa. No algal constructions were encountered in the Anchor Bay outcrop; instead, we observed mixed coralline algae and larger benthic foraminifera (LBF) grainstone to rudstone, also alternating with mudstone to wackestone (Figure 3d). Bivalve and echinoid fragments are present in all of these facies. At Anchor Bay, channels are present between 4 m and 9.5 m above the base of the section (Figure 3e); these are filled with a mixture of intraclasts (grainstone to wackestone); serpulids (Figure 3f) are located at the bottom and walls of some of the channels.

Mixed coralline algae and LBF packstone to grainstone mark the middle part of the UCL at Rдум Majjiesa, Santi and Anchor Bay. Planar and hummocky cross-stratification can be identified in Anchor Bay and Rдум Majjiesa. Above this part, coarser-grained facies (bindstone/bafflestone) are observed in these outcrops. At Rдум Majjiesa, one horizon with corals (*Porites?*) was encountered ~15m above the base of the section in poor exposure conditions. The top of the section at Santi is an oyster-rich horizon, also containing limpets (Figure 3g). Meanwhile, at Rдум Majjiesa (Figure 3h) and Bobbyland (Figure 3i), the top of the unit was comprised of cross stratified coralline algae and LBF packstone to grainstone. The mode of cross-stratification alternates (Figure 3h) and includes herringbone, planar and hummocky cross-stratification.

The deposition geometry at the outcrops level is poorly expressed. Beds appear to be relatively continuous along a northwest-southeast trend but less so in the perpendicular direction. Where cross-stratification was observed, both the herringbone and the planner stratification were oriented north-east to south-west. In none of the surveyed site were lateral transitions of the coralline facies observed. Some outcrops exhibit well-pronounced clinofolds, either as small bedding scale features dipping to the north to northeast as observed at Rдум Majjiesa (Figure 4a-b), or large scale clinofolds dipping towards the north to the northwest as observed at Mellieħa (Figure 4c-d). At Rдум Majjiesa, these clinofolds were comprised of rhodolites, coralline nodules, coralline or LBF sand.

The transition from the Greensand unit to the UCL is gradual, occurring over an interval of 0.3 to 1.0 cm, from coarse sand to silt to fine sand. The colour also changes along this transition, from green to white/cream. Above this bed, the lower part of the UCL succession is dominated by coralline algae material. The lower 7 m in Santi and Ghajn Tuffieħa, as well as the lower 5 m in Rдум Majjiesa (Figure 2), are comprised of alternating crustose coralline algae (CCA) bindstone (Figures 3a & 3b), and rhodolithic bafflestone to floatstone (Figure 3c) interbedded with fine-grained mudstone to wackestone. The rhodoliths are 5 to 10 cm in diameter, and are for the most part spherical and well-rounded; smaller (0.5 to 2 cm) coralline nodules are present and bound in the CCA beds. Solitary corals were also encountered in some cases. Some fragmentation of



**Figure 3:** Facies occurrence in the UCL: a. alternating bafflestone layers and mudstone to wackestone, Ghajn Tuffieha; b. alternating bindstone and wackestone, Ghajn Tuffieha; c. rhodolithic floatstone, Santi; d. alternating packstone and grainstone layers, Anchor Bay; e. channel fill conglomerate (lithoclastic floatstone, clasts comprised of grainstone); Anchor Bay; f. sepiolitic bafflestone, Anchor Bay; g. Limpet on background of a packstone layer, Santi; h. imbricated lithoclastic (clasts comprised of grainstone) floatstone, Bobbyland. White scale bar, 10cm, black scale bar 1cm.

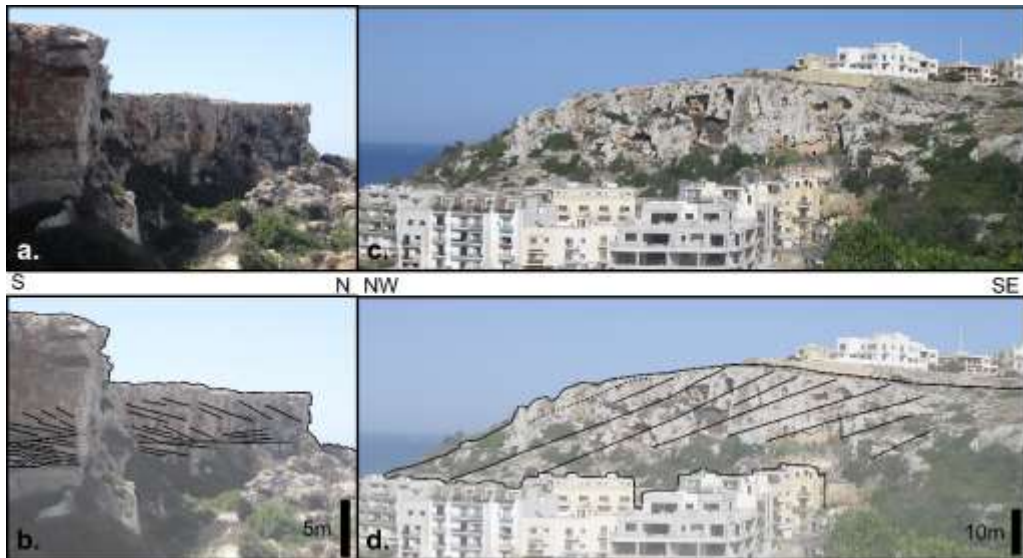


**Figure 4:** Large scale sedimentary features in the UCL. a. (original photos) and b. (bedding highlights) show large inclined bedding at Rđum Majjiesa. c. (original photos) and d. (bedding highlights) shows large scale clinoforms at Mellieħa.

## Seismic reflection data

Within the designated study interval, five seismic facies were identified. SF1 - High amplitude continuous reflections with downlap or onlap configuration; SF2 – chaotic low amplitude reflections; SF3 – low to medium amplitude inclined, clinoform-like reflections, often expressing downlap; SF4 – low to medium amplitude sub-horizontal non-continuous reflections, often exhibiting ponding and onlap geometries; SF5 – medium amplitude horizontal to sub-horizontal continuous reflections.

The seismic facies relations are best represented along a shore-parallel transect between the islands (Figure 5). SF5 characterizes the lower part of the investigated interval. It terminates to the south by a truncation and to the north by a pronounced strong reflection. The extent of this facies was delineated as SU1 (Figure 5b). Above this unit are lateral transition between SF2, SF3 and SF4 (Figure 5c), capped by a pronounced reflection above which this pattern is repeated. These lateral elements were delineated as SU2 and SU3, with the SF2 and SF3 as the “a” subunit and SF4 as the “b” subunit. All units are truncated by a strong reflection above which SF1 is dominant; this was selected as the base of SU4, which extends above it until the seafloor. Unit thickness is not consistent, increasing between the islands and decreasing towards the shore, and conform to the horst and graben structure (Figure 6). The inter-island area includes grabens (Figure 6b) with thickness increasing towards the centre and decreasing towards the margins. The base of SF1 and top of SF5 rises towards the landmasses (Figures S2 and S3) illustrating these trends.

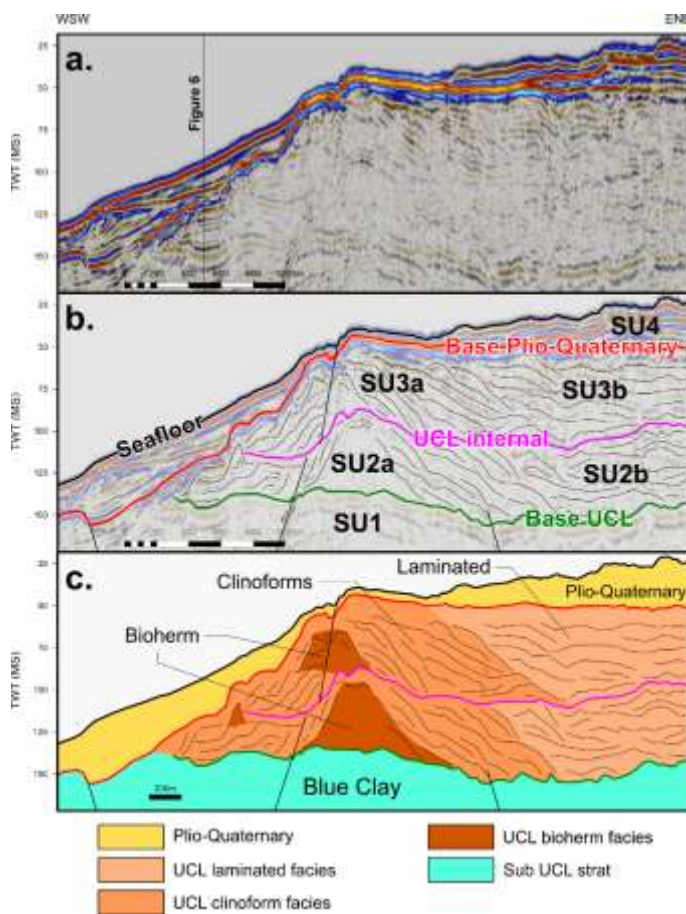


**Figure 5:** Uninterpreted (a) delineated (b) and interpreted (c) time migrated section (a), line MGT16\_77 trending approximate WSW-ENE. Seismic facies are shown in c. SF1 in yellow, SF2 in dark orange, SF3 in light orange SF4 in pink and SF5 in blue.

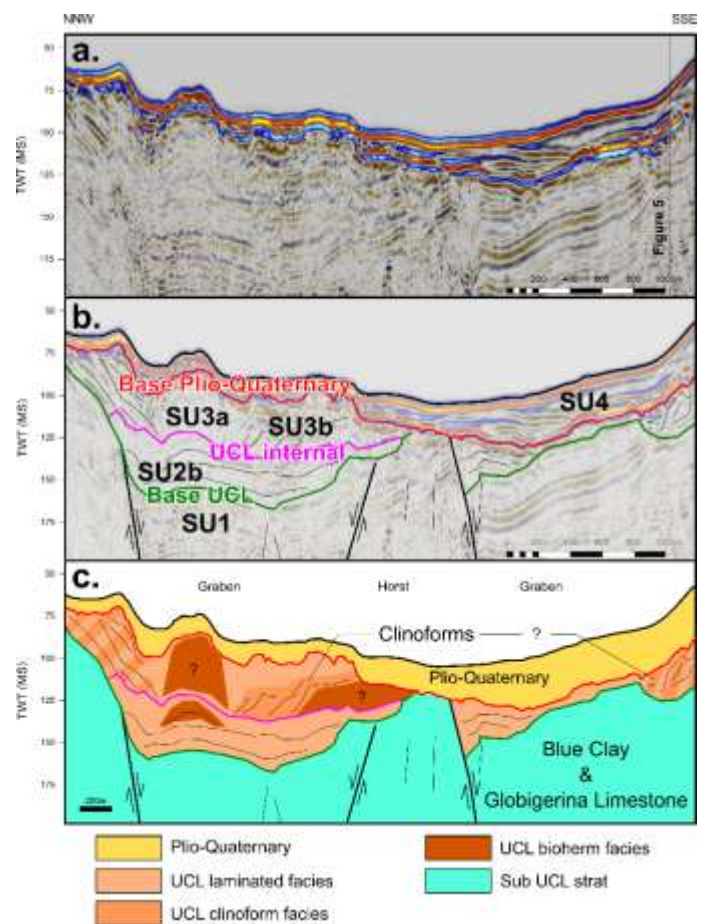


**Figure 6:** Uninterpreted (a) delineated (b) and interpreted (c) time migrated section (a), line MGT16\_106 trending approximate NNW-SSE. Seismic facies are shown in c. SF1 in yellow, SF2 in dark orange, SF3 in light orange and SF4 in blue.

## Interpretation

### Outcrops

Both coralline bindstone and bafflestone to floatstone are indicative of deposition within the photic range of the water column, although they can reach into the mesophotic depth, and are not substantially affected by salinity or temperature (Adey and Macintyre, 1973; Kahng et al., 2010). Prior studies (Bosence and Pedley, 1982; Pedley, 1979, 1978) had identified the primary algae encruster as *Lithophyllum* and *Mesophyllum*, with encrusting foraminifera and bryozoans also present. The alternation of coralline bindstone and rhodoliths suggests variation in water agitation as rhodoliths are formed in an environment with more disruption (Williams et al., 2018). The high sphericity of the rhodoliths also points to a higher energy setting (Aguirre et al., 2017). The fragmentation of the rhodoliths within the lower parts of the section in Santi and Ghajn Tuffieħa point to a relatively energetic environment, although the presence of fine grains in all localities suggests that energy is intermittent. In localities not dominated by coralline algae construction (e.g. Anchor Bay, Bobbyland), coralline material is being transported in addition to LBF. It is unclear if the channels observed in Anchor Bay are purely subaqueous, although the absence of exposure-related features appears to support this interpretation. Given the occurrence of large grain fill, it is most likely that they represent a high energy environment, possibly of the shallow sublittoral. These all point to a wide energy range across the deposition of the UCL, spatially as well as temporally.

Fauna present within this upper portion of the unit, such as limpets, suggest a littoral to sublittoral position (Meadows and Campbell, 1972). This interpretation is also supported by the presence of herringbone cross-stratification in Rđum Majjiesa, indicating intertidal conditions (Nichols, 2009). This interplay with hummocky and planar cross-stratification indicates a relatively shallow and energetic environment but with significantly more turbidity, which limited the ability of coralline algae to colonize. Pedley (1979) noted that the coralline bioherms would have generated a patchwork of different energy states around them, which would allow for varying energy state over a short distance until topography is filled. While there are some bioherm construction and accretion of coralline bindstone (Figure 3b), both laterally and vertically, it is mostly local. The larger-scale structure observed at the outcrop-level (Figure 4) points to lateral distribution of material with periods marked by progradation.

With this in mind, the alternation in accretion mode of the coralline algae between bindstone and rhodoliths, and the interruptions of finer grain layers between the coralline horizons (Figure 2), may be interpreted as short term depositional cycles, either autocyclic or allocyclic, developing by the interaction between production by the calcifying factory and accommodation space. While effects like storms and variation in runoff could disrupt coralline accumulation (Dulin et al., 2020), no storm deposits were encountered. Malta, being an isolated platform, would have limited potential for runoff.

These smaller cycles integrate into two larger-scale cycles, which could be inferred from their accretion pattern. The occurrence of coastal and littoral deposits, serpulids and corals help identify key surfaces bounding these cycles. This is in line with prior studies by Pedley (1996, 1979, 1976) and Cornée et al. (2004); the latter, in particular, noted the termination of the corals as a major transgressive surface. The top of the second cycle as encountered in both Bobbyland and Rđum Majjiesa is defined by cross-bedded grainstone with coastal characteristics; this is not the case for the first cycle, which exhibit a more complex pattern. In addition, the second cycle was not encountered in all locations, suggesting it was eroded or was not emplaced at all. These elements suggest that the termination of the second cycle occurred with less available accommodation space than the first cycle.

## Seismic reflection data

SU4 overlays a significant unconformity and exhibits a significant shift in seismic facies. Based on existing knowledge of the configuration of deposits on the Maltese platform (Gatt, 2007; Max et al., 1993; Micallef et al., 2011; Osler and Algan, 1999), the deposits of SU4 are most likely Plio-Quaternary and the base of this unit is an unconformity related to the MSC (Messinian erosional surface) or the subsequent Zanclean megaflood (Garcia-Castellanos et al., 2020). The underlying SU3 would therefore be part of the UCL. The unit is truncated, and its thickness decreases to 0 to the south-west (Figure S4).

The lateral continuation from SF2 to SF4 (Figure 5c) observed in both SU3 and SU2 point to similar depositional systems in both units. The morphology observed by SF2 is consistent with the seismic character of a carbonate buildup (Burgess et al., 2013). Its position relative to the Islands also suggests these structure could be the lateral continuation of the UCL main bioherms observed in the outcrops (Pedley, 1979, 1976). As such SF2 is interpreted as a bioherm, which would suggest that both SU3 and SU2 combined are the equivalent of the UCL, with each unit representing a depositional cycle. The maximum thickness of this combined unit is ~100 m, which is comparable to the maximum thickness of ~80 m reported by Corn e et al. (2004) for the UCL. By extension, SF3 would probably mark largescale clinofolds spilling off the main bioherm, as observed onshore (Figure 4), and SF4 would be a protected environment behind the outer bioherms. The onlap contact of SF4 suggests that this facies was deposited in the later part of the depositional cycle, filling up available accommodation space. Schlager (2005) defined the C type carbonate factory as one dominated by material from a biological source rich in heterotrophic organisms, larger benthic foraminifera and coralline algae. This differs from the type of carbonate production in tropical carbonate platform (also called T factory). Whereas in the T factory construction is for the most part of a ridged framework, in the C type factory typically produces skeletal hash of sand-to-granule size grains. Grain generation in a coralline dominated C type factory, such as the UCL, would be a significant contributor to its immediate environment, although the position and main production zone might move laterally in response to change in sea level.

The underlying horst and graben structure of the Maltese Archipelago (Dart et al., 1993) predated the deposition of the UCL, and the offshore deposit conforms to the pre-existing structure (Figure 6). This may suggest that the deposits observed in the seismic reflection data were deposited in a lower topographic position, with possible overspill from Malta and Gozo observed on the margins of the grabens (Figure 6c). This would point to the fill by SF4 to be a lateral transport for a migrated main production zone with the increasing water level.

Finally, SU1 contains within it the pre-UCL units that include the Globigerina Limestone, Blue Clay and Greensand. Given that the thickness of the Greensand is only a few meters (Pedley, 1978), it is probably not observed in the seismic data and/or incorporated in the Base UCL horizon. Therefore the upper part of SU 1 is considered to be the Blue Clay formation.

## Discussion

The most recent model of global sea-level change in the late Miocene (Miller et al., 2020) depicts a base level rise of ~20 m in the late Tortonian (~8 to 7.5 Ma, Figure 7). After this rise, mean sea level remained relatively static until the MSC. Baldassini and Di Stefano (2017) inferred that the age of the base of the Upper Coralline Limestone is at ~8 Ma and the top of it lies within the MNN11 nanofossil zone. Dolomitization appears to have occurred wherever such interaction took place (de Lange and Krijgsman, 2010; Manzi et al., 2011; Sabino et al., 2020). However, no dolomite was detected in the mineralogical analysis, suggesting minimal interaction of hypersaline MSC waters with any of the Maltese deposits. This limits the age of the top of the UCL to no more ~6 Ma. The emplacement of a shallow water unit atop a

deepwater unit such as the Blue Clay formation (Abels et al., 2005), while sea level was rising, already suggests a major uplift of the Maltese barrier during the late Miocene. By examining the  $^{87}\text{Sr}/^{86}\text{Sr}_{\text{carbonate}}$  record of the Eastern Mediterranean at the time (Figure 7; Flecker and Ellam, 2006; Schildgen et al., 2014), we note that they exhibit significantly lower values when compared with the coeval oceanic reference value (McArthur et al., 2001). Lower values are also observed in the central Mediterranean (Kocsis et al., 2008; Schildgen et al., 2014; Sprovieri et al., 2004), but these are no lower than 0.70887, while the samples in the Eastern Mediterranean can be lower than 0.70880. These values are still higher than the departure observed during the MSC (Flecker et al., 2002; Müller and Mueller, 1991; Roveri et al., 2014b), but the trend is in the same direction. Overall the  $^{87}\text{Sr}/^{86}\text{Sr}$  ratio of the ocean is governed by the balance between continental weathering and hydrothermal supply from mid-ocean ridges (Jones et al., 1994). However, in a restricted basin, the contribution from terrestrial sources may overprint the oceanic signal. Combining these two lines of evidence, we suggest a restriction of exchange between the Eastern and Western Mediterranean due to uplift of the terrain between Sicily and Tunisia. This uplift appears to have been driven by the aftermath of the collision between the African margin and the Sicilian block (Jongsma et al., 1985), with a total uplift of >500m during the Tortonian to the earliest Pliocene (Yellin-Dror et al., 1997). No clear indication of such movement is observed in the seismic data available for this study. Paleodepth estimation at the top of the Blue Clay formation (Serravallian) is estimated at 150 to 200m (Digeronimo et al., 1981; Jacobs et al., 1996), while in the upper part of the UCL (upper Messinian) we identified coastal to littoral deposits. Considering that the total thickness of the UCL deposits is <30m, the filling of accommodation space alone could not account for these observations. The total accommodation is also offset but ~25m of sea-level rise during the deposition of the UCL (Miller et al., 2020, Figure 7), suggesting an uplift of at least 150m in Malta.

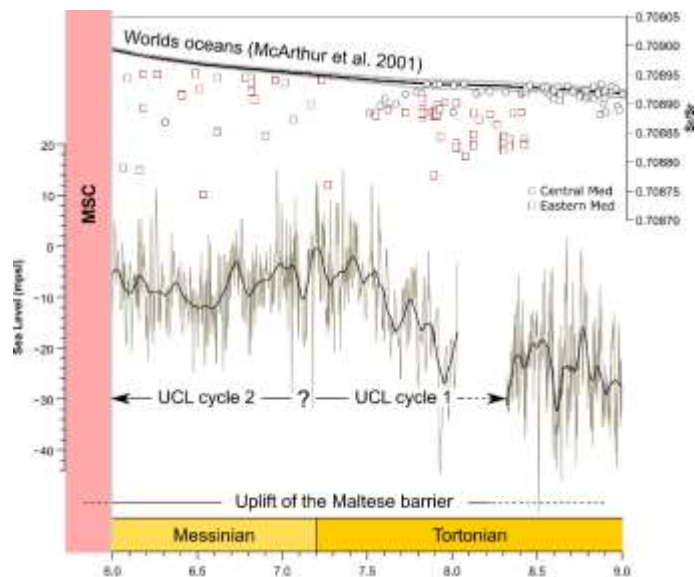


**Figure 7:** Temporal context of the deposition of the UCL, Sr isotopes record of the Eastern (Flecker and Ellam, 2006; Schildgen et al., 2014) and Central (Kocsis et al., 2008; Schildgen et al., 2014; Sprovieri et al., 2004) Mediterranean relative to the coeval oceanic reference (McArthur et al., 2001). Global sea level (Miller et al., 2020) and proposed relation to the deposition of the UCL cycles.

governed by a 1.2 Ma eccentricity modulated astronomical frequencies, and represent two 3<sup>rd</sup> order cycles (Boulila et al., 2012). This overall trend of fill points to limited accommodation space generation, facilitated only by the coeval sea level rise (Figure 7), as well as possibly by local tectonics forming local basins. This

Our observations point to the emplacement of two cycles of shallow-water deposits in the UCL formation terminating near sea level, indicating that accommodation space was available for the establishment of two depositional cycles and topography fill by a carbonate factory. Each cycle (Figure 5) begins with the local establishment of bioherms, which grow vertically with a lateral component (aggradation-progradation), followed by a phase of lateral growth (progradation) and finally a stage of accommodation fill (aggradation). The initial two phases would be comparable to the initial shallowing upwards phase observed in the outcrops, with the aggradational phases being comparable to the deepening upwards phase. The available timeframe of emplacement of the UCL (from ~8 to ~6 Ma), and the known eustatic sea-level patterns (Miller et al., 2020), suggest that the depositional cycles are of the order of 1 Ma each, likely

is evident by the conformity of the sediment to the normal faults observed in the seismic data (Figure 6). The overall stress field at the time would have been a compressional one along a north-south vector due to collision. This compression generated an extensional regime along an east-west vector in the late Miocene and early Pliocene (Civile et al., 2008). This trend was further enhanced by coeval rifting along this direction (Belguith et al., 2013; Corti et al., 2006). While this process would have generated local basins, the overall effect would have been to magnify the total uplift of the barrier.

## Conclusions

Over the late Miocene, the area around the Maltese Archipelago has experienced a significant uplift. This uplift raised the Maltese Islands to a water depth that allowed the emplacement of a shallow-water carbonate unit in the form of the Upper Coralline Limestone formation. This unit was deposited during two depositional cycles, both with a strong trend of accommodation space fill. The mode of emplacement and overall geometry suggests a very shallow position of the Malta Plateau, conforming to an existing tectonic structure already present in the late Miocene. This uplift appears to have played a role in restricting connectivity of the water masses between the east and west Mediterranean prior to the onset of the MSC. This could have played an important role in triggering halite deposition in the larger eastern basin prior to salt deposition in the Western Basin. This uplift would have restricted flow to the eastern basin at a time when the western basin was still relatively well connected to the Atlantic Ocean and could have played a pivotal role in the observed differences in deposits between the two basins during the MSC.

## Acknowledgements

This study was conducted as part of the first author's Marie Skłodowska Curie fellowship (101003394 — RhodoMalta). A.M. is funded by the European Research Council (ERC) under the European Union's Horizon 2020 Programme grant agreement No. 677898 (MARCAN). Initial fieldwork was funded by a STSM awarded to OMB as part of the MEDSALT (CA15103) COST Action. We are grateful to Infrastructure Malta for providing access to their data. The field and oceanographic surveys were possible following permits issued by the Maltese authorities. Special thanks is extended to Daniel Sultana for the useful discussions and to Nicolas Waldmann for introduction between the authors. Schlumberger is thanked for use of the Petrel E&P Software.

## References

- Abels, H.A., Hilgen, F.J., Krijgsman, W., Kruk, R.W., Raffi, I., Turco, E., Zachariasse, W.J., 2005. Long-period orbital control on middle Miocene global cooling: Integrated stratigraphy and astronomical tuning of the Blue Clay Formation on Malta. *Paleoceanography* 20, PA4012. <https://doi.org/10.1029/2004PA001129>
- Adam, J., Reuther, C.-D., Grasso, M., Torelli, L., 2000. Active fault kinematics and crustal stresses along the Ionian margin of southeastern Sicily. *Tectonophysics* 326, 217–239. [https://doi.org/10.1016/S0040-1951\(00\)00141-4](https://doi.org/10.1016/S0040-1951(00)00141-4)
- Adey, W.H., Macintyre, I.G., 1973. Crustose Coralline Algae: A Re-evaluation in the Geological Sciences. *Geol. Soc. Am. Bull.* 84, 883. [https://doi.org/10.1130/0016-7606\(1973\)84<883:CCAARI>2.0.CO;2](https://doi.org/10.1130/0016-7606(1973)84<883:CCAARI>2.0.CO;2)
- Aguirre, J., Braga, J.C., Bassi, D., 2017. Rhodoliths and Rhodolith Beds in the Rock Record, in: Riosmena-Rodríguez, R. (Ed.), *Rhodolith/Maërl Beds: A Global Perspective*. Springer, Coastal Research Library 15, pp. 105–138. [https://doi.org/10.1007/978-3-319-29315-8\\_5](https://doi.org/10.1007/978-3-319-29315-8_5)

- Baldassini, N., Di Stefano, A., 2017. Stratigraphic features of the Maltese Archipelago: a synthesis. *Nat. Hazards* 86, 203–231. <https://doi.org/10.1007/s11069-016-2334-9>
- Belguith, Y., Geoffroy, L., Mourgues, R., Rigane, A., 2013. Analogue modelling of Late Miocene–Early Quaternary continental crustal extension in the Tunisia–Sicily Channel area. *Tectonophysics* 608, 576–585. <https://doi.org/10.1016/j.tecto.2013.08.023>
- Ben-Avraham, Z., Nur, A., Giuseppe, C., 1987. Active transcurrent fault system along the north African passive margin. *Tectonophysics* 141, 249–260. [https://doi.org/10.1016/0040-1951\(87\)90189-2](https://doi.org/10.1016/0040-1951(87)90189-2)
- Blanc, P.-L., 2000. Of sills and straits: a quantitative assessment of the Messinian Salinity Crisis. *Deep Sea Res. Part I Oceanogr. Res. Pap.* 47, 1429–1460. [https://doi.org/10.1016/S0967-0637\(99\)00113-2](https://doi.org/10.1016/S0967-0637(99)00113-2)
- Blanc, P.L., 2006. Improved modelling of the Messinian Salinity Crisis and conceptual implications. *Palaeogeogr. Palaeoclimatol. Palaeoecol.* 238, 349–372. <https://doi.org/10.1016/j.palaeo.2006.03.033>
- Borrelli, M., Perri, E., Critelli, S., Gindre-Chanu, L., 2020. The onset of the Messinian Salinity Crisis in the central Mediterranean recorded by pre-salt carbonate/evaporite deposition. *Sedimentology* sed.12824. <https://doi.org/10.1111/sed.12824>
- Bosence, D.W.J., Pedley, H.M., 1982. Sedimentology and palaeoecology of a Miocene coralline algal biostrome from the Maltese Islands. *Palaeogeogr. Palaeoclimatol. Palaeoecol.* 38, 9–43. [https://doi.org/10.1016/0031-0182\(82\)90062-1](https://doi.org/10.1016/0031-0182(82)90062-1)
- Boulila, S., Galbrun, B., Laskar, J., Pälike, H., 2012. A ~9myr cycle in Cenozoic  $\delta$  13C record and long-term orbital eccentricity modulation: Is there a link? *Earth Planet. Sci. Lett.* 317–318, 273–281. <https://doi.org/10.1016/j.epsl.2011.11.017>
- Buchbinder, B., 1996. Miocene carbonates of the Eastern Mediterranean, the Red Sea and the Mesopotamian Basin: geodynamic and eustatic controls, in: Franseen, E.K., Esteban, M., Ward, W.C., Rouchy, J.-M. (Eds.), *Models for Carbonate Stratigraphy from Miocene Reef Complexes of Mediterranean Regions*. *SEPM Concepts in sedimentology and paleontology* 5, pp. 333–345. <https://doi.org/10.2110/csp.96.01.0317>
- Burgess, P.M., Winefield, P., Minzoni, M., Elders, C., 2013. Methods for identification of isolated carbonate buildups from seismic reflection data. *Am. Assoc. Pet. Geol. Bull.* 97, 1071–1098. <https://doi.org/10.1306/12051212011>
- Catanzariti, R., Gatt, M., 2014. Calcareous nannofossil biostratigraphy from the middle / late Miocene of Malta and Gozo ( Central Mediterranean ) 11, 303–336.
- Civile, D., Lodolo, E., Tortorici, L., Lanzafame, G., Brancolini, G., 2008. Relationships between magmatism and tectonics in a continental rift: The Pantelleria Island region (Sicily Channel, Italy). *Mar. Geol.* 251, 32–46. <https://doi.org/10.1016/j.margeo.2008.01.009>
- Cornée, J.J., Saint Martin, J.P., Conesa, G., Münch, P., André, J.P., Saint Martin, S., Roger, S., 2004. Correlations and sequence stratigraphic model for Messinian carbonate platforms of the western and central Mediterranean. *Int. J. Earth Sci.* 93, 621–633. <https://doi.org/10.1007/s00531-004-0400-0>
- Corti, G., Cuffaro, M., Doglioni, C., Innocenti, F., Manetti, P., 2006. Coexisting geodynamic processes in the Sicily Channel. *Spec. Pap. Geol. Soc. Am.* 409, 83–96. [https://doi.org/10.1130/2006.2409\(05\)](https://doi.org/10.1130/2006.2409(05))
- Dart, C.J., Bosence, W.J., McClay, K.R., 1993. Stratigraphy and structure of the Maltese graben system. *J. Geol. Soc. London* 150, 1153–1166. <https://doi.org/DOI.10.1144/gsjgs.150.6.1153>

- de Lange, G.J., Krijgsman, W., 2010. Messinian salinity crisis: A novel unifying shallow gypsum/deep dolomite formation mechanism. *Mar. Geol.* 275, 273–277. <https://doi.org/10.1016/j.margeo.2010.05.003>
- Digeronimo, I., Grasso, M., Pedley, H.M., 1981. Palaeoenvironment and palaeogeography of Miocene marls from southeast Sicily and the Maltese Islands. *Palaeogeogr. Palaeoclimatol. Palaeoecol.* 34, 173–189. [https://doi.org/10.1016/0031-0182\(81\)90063-8](https://doi.org/10.1016/0031-0182(81)90063-8)
- Dulin, T., Avnaim-Katav, S., Sisma-Ventura, G., Bialik, O.M., Angel, D.L., 2020. Rhodolith beds along the southeastern Mediterranean inner shelf: Implications for past depositional environments. *J. Mar. Syst.* 201, 103241. <https://doi.org/10.1016/j.jmarsys.2019.103241>
- Dunham, R.J., 1962. Classification of Carbonate Rocks According to Depositional Textures, in: Ham, W.E. (Ed.), *Classification of Carbonate Rocks - A Symposium*. AAPG Memoir 1, pp. 108–121.
- Embry, A.F., Klovan, J.E., 1971. A Late Devonian reef tract on northeastern Banks Island, NWT. *Bull. Can. Pet. Geol.* 19, 730–781.
- Flecker, R., De Villiers, S., Ellam, R.M., 2002. Modelling the effect of evaporation on the salinity-<sup>87</sup>Sr/<sup>86</sup>Sr relationship in modern and ancient marginal-marine systems: The Mediterranean Messinian Salinity Crisis. *Earth Planet. Sci. Lett.* 203, 221–233. [https://doi.org/10.1016/S0012-821X\(02\)00848-8](https://doi.org/10.1016/S0012-821X(02)00848-8)
- Flecker, R., Ellam, R.M.M., 2006. Identifying Late Miocene episodes of connection and isolation in the Mediterranean–Paratethyan realm using Sr isotopes. *Sediment. Geol.* 188–189, 189–203. <https://doi.org/10.1016/j.sedgeo.2006.03.005>
- Garcia-Castellanos, D., Micallef, A., Estrada, F., Camerlenghi, A., Ercilla, G., Periañez, R., Abril, J.M., 2020. The Zanclean megaflood of the Mediterranean – Searching for independent evidence. *Earth-Science Rev.* 201, 103061. <https://doi.org/10.1016/j.earscirev.2019.103061>
- Gardiner, W., Grasso, M., Sedgely, D., 1995. Plio-pleistocene fault movement as evidence for mega-block kinematics within the Hyblean—Malta Plateau, Central Mediterranean. *J. Geodyn.* 19, 35–51. [https://doi.org/10.1016/0264-3707\(94\)00006-9](https://doi.org/10.1016/0264-3707(94)00006-9)
- Gatt, P.A., 2007. Controls on Plio-Quaternary foreland sedimentation in the region of the Maltese Islands. *Boll. della Soc. Geol. Ital.* 126, 119–129.
- Gatt, P.A., Gluyas, J.G., 2012. Climatic controls on facies in Palaeogene Mediterranean subtropical carbonate platforms. *Pet. Geosci.* 18, 355–367. <https://doi.org/10.1144/1354-079311-032>
- Gutscher, M.-A., Dominguez, S., de Lepinay, B.M., Pinheiro, L., Gallais, F., Babonneau, N., Cattaneo, A., Le Faou, Y., Barreca, G., Micallef, A., Rovere, M., 2016. Tectonic expression of an active slab tear from high-resolution seismic and bathymetric data offshore Sicily (Ionian Sea). *Tectonics* 35, 39–54. <https://doi.org/10.1002/2015TC003898>
- Haq, B., Gorini, C., Baur, J., Moneron, J., Rubino, J.-L., 2020. Deep Mediterranean’s Messinian evaporite giant: How much salt? *Glob. Planet. Change* 184, 103052. <https://doi.org/10.1016/j.gloplacha.2019.103052>
- Hsü, K., Ryan, W., Cita, M., 1973. Late Miocene desiccation of the Mediterranean. *Nature* 242, 240–244.
- Jacobs, E., Weissert, H., Shields, G., Stille, P., 1996. The Monterey Event in the Mediterranean: A record from shelf sediments of Malta. *Paleoceanography* 11, 717–728. <https://doi.org/10.1029/96PA02230>
- Jones, C.E., Jenkyns, H.C., Coe, A.L., Stephen, H.P., 1994. Strontium isotopic variations in Jurassic and

- Cretaceous seawater. *Geochim. Cosmochim. Acta* 58, 3061–3074. [https://doi.org/10.1016/0016-7037\(94\)90179-1](https://doi.org/10.1016/0016-7037(94)90179-1)
- Jongsma, D., van Hinte, J.E., Woodside, J.M., 1985. Geologic structure and neotectonics of the North African Continental Margin south of Sicily. *Mar. Pet. Geol.* 2, 156–179. [https://doi.org/10.1016/0264-8172\(85\)90005-4](https://doi.org/10.1016/0264-8172(85)90005-4)
- Kahng, S.E., Garcia-Sais, J.R., Spalding, H.L., Brokovich, E., Wagner, D., Weil, E., Hinderstein, L., Toonen, R.J., 2010. Community ecology of mesophotic coral reef ecosystems. *Coral Reefs* 29, 255–275. <https://doi.org/10.1007/s00338-010-0593-6>
- Kocsis, L., Vennemann, T.W., Fontignie, D., Baumgartner, C., Montanari, A., Jelen, B., 2008. Oceanographic and climatic evolution of the Miocene Mediterranean deduced from Nd, Sr, C, and O isotope compositions of marine fossils and sediments. *Paleoceanography* 23, 1–20. <https://doi.org/10.1029/2007PA001540>
- Kontakiotis, G., Besiou, E., Antonarakou, A., Zarkogiannis, S.D., Kostis, A., Mortyn, P.G., Moissette, P., Cornée, J.J., Schulbert, C., Drinia, H., Anastasakis, G., Karakitsios, V., 2019. Decoding sea surface and paleoclimate conditions in the eastern Mediterranean over the Tortonian-Messinian Transition. *Palaeogeogr. Palaeoclimatol. Palaeoecol.* 534, 109312. <https://doi.org/10.1016/j.palaeo.2019.109312>
- Kouwenhoven, T.J., Morigi, C., Negri, A., Giunta, S., Krijgsman, W., Rouchy, J.M., 2006. Paleoenvironmental evolution of the eastern Mediterranean during the Messinian: Constraints from integrated microfossil data of the Pissouri Basin (Cyprus). *Mar. Micropaleontol.* 60, 17–44. <https://doi.org/10.1016/j.marmicro.2006.02.005>
- Krijgsman, W., Blanc-Valleron, M.M., Flecker, R., Hilgen, F.J., Kouwenhoven, T.J., Merle, D., Orszag-Sperber, F., Rouchy, J.M., 2002. The onset of the Messinian salinity crisis in the Eastern Mediterranean (Pissouri Basin, Cyprus). *Earth Planet. Sci. Lett.* 194, 299–310. [https://doi.org/10.1016/S0012-821X\(01\)00574-X](https://doi.org/10.1016/S0012-821X(01)00574-X)
- Manzi, V., Lugli, S., Roveri, M., Schreiber, B.C., Gennari, R., 2011. The Messinian “Calcare di Base” (Sicily, Italy) revisited. *Bull. Geol. Soc. Am.* 123, 347–370. <https://doi.org/10.1130/B30262.1>
- Max, M.D., Kristensen, E., Michelozzi, E., 1993. Small scale Plio-Quaternary sequence stratigraphy and shallow geology of the west-central Malta Plateau, in: Max, M.D., Colantoni, P. (Eds.), *UNESCO Technical Reports in Marine Science*. Urbino, pp. 117–122.
- McArthur, A.J.M., Howarth, R.J., Bailey, T.R., McArthur, J.M., Howarth, R.J., Bailey, T.R., 2001. Strontium Isotope Stratigraphy: LOWESS Version 3: Best Fit to the Marine Sr-Isotope Curve for 0–509 Ma and Accompanying Look-up Table for Deriving Numerical Age. *J. Geol.* 109, 155–170. <https://doi.org/10.1086/319243>
- Meijer, P.T., 2006. A box model of the blocked-outflow scenario for the Messinian Salinity Crisis. *Earth Planet. Sci. Lett.* 248, 486–494. <https://doi.org/10.1016/j.epsl.2006.06.013>
- Meilijson, A., Hilgen, F., Sepúlveda, J., Steinberg, J., Fairbank, V., Flecker, R., Waldmann, N.D., Spaulding, S.A., Bialik, O.M., Boudinot, F.G., Illner, P., Makovsky, Y., 2019. Chronology with a pinch of salt: Integrated stratigraphy of Messinian evaporites in the deep Eastern Mediterranean reveals long-lasting halite deposition during Atlantic connectivity. *Earth-Science Rev.* 194, 374–398. <https://doi.org/10.1016/j.earscirev.2019.05.011>
- Meilijson, A., Steinberg, J., Hilgen, F., Bialik, O.M., Waldmann, N.D., Makovsky, Y., 2018. Deep-basin evidence resolves a 50-year-old debate and demonstrates synchronous onset of Messinian evaporite deposition in a non-desiccated Mediterranean. *Geology* 46. <https://doi.org/10.1130/G39868>

- Micallef, A., Berndt, C., Debono, G., 2011. Fluid flow systems of the Malta Plateau, Central Mediterranean Sea. *Mar. Geol.* 284, 74–85. <https://doi.org/10.1016/j.margeo.2011.03.009>
- Micallef, A., Georgiopoulou, A., Mountjoy, J., Huvenne, V.A.I., Iacono, C. Lo, Le Bas, T., Del Carlo, P., Otero, D.C., 2016. Outer shelf seafloor geomorphology along a carbonate escarpment: The eastern Malta Plateau, Mediterranean Sea. *Cont. Shelf Res.* 131, 12–27. <https://doi.org/10.1016/j.csr.2016.11.002>
- Miller, K.G., Browning, J. V., Schmelz, W.J., Kopp, R.E., Mountain, G.S., Wright, J.D., 2020. Cenozoic sea-level and cryospheric evolution from deep-sea geochemical and continental margin records. *Sci. Adv.* 6, eaaz1346. <https://doi.org/10.1126/sciadv.aaz1346>
- Moissette, P., Cornée, J.J., Antonarakou, A., Kontakiotis, G., Drinia, H., Koskeridou, E., Tsourou, T., Agiadi, K., Karakitsios, V., 2018. Palaeoenvironmental changes at the Tortonian/Messinian boundary: A deep-sea sedimentary record of the eastern Mediterranean Sea. *Palaeogeogr. Palaeoclimatol. Palaeoecol.* 505, 217–233. <https://doi.org/10.1016/j.palaeo.2018.05.046>
- Müller, D.W., Mueller, P.A., 1991. Origin and age of the Mediterranean Messinian evaporites: implications from Sr isotopes. *Earth Planet. Sci. Lett.* 107, 1–12. [https://doi.org/10.1016/0012-821X\(91\)90039-K](https://doi.org/10.1016/0012-821X(91)90039-K)
- Osler, J.C., Algan, O., 1999. A high resolution seismic sequence analysis of the Malta Plateau.
- Pedley, H.M., 2011. The Calabrian Stage, Pleistocene highstand in Malta: a new marker for unravelling the Late Neogene and Quaternary history of the islands. *J. Geol. Soc. London.* 168, 913–926. <https://doi.org/10.1144/0016-76492010-080>
- Pedley, H.M., 1996. Miocene reef facies of the Pelagian region (central Mediterranean), in: *Models for Carbonate Stratigraphy from Miocene Reef Complexes of Mediterranean Regions*. SEPM (Society for Sedimentary Geology), pp. 247–259. <https://doi.org/10.2110/csp.96.01.0247>
- Pedley, H.M., 1979. Miocene bioherms and associated structures in the Upper Coralline limestone of the Maltese Islands: their lithification and palaeoenvironment. *Sedimentology* 26, 577–591. <https://doi.org/10.1111/j.1365-3091.1979.tb00930.x>
- Pedley, H.M., 1978. A new lithostratigraphical and palaeoenvironmental interpretation for the coralline limestone formations (Miocene) of the Maltese Islands. *Overseas Geol. Miner. Resour.* 54, 1–17.
- Pedley, H.M., 1976. A palaeoecological study of the Upper Coralline Limestone, Terebratula-Aphelesia bed (miocene, Malta) based on bryozoan growth-form studies and brachiopod distributions. *Palaeogeogr. Palaeoclimatol. Palaeoecol.* 20, 209–234. [https://doi.org/10.1016/0031-0182\(76\)90003-1](https://doi.org/10.1016/0031-0182(76)90003-1)
- Reuther, C.-D., Ben-Avraham, Z., Grasso, M., 1993. Origin and role of major strike-slip transfers during plate collision in the central Mediterranean. *Terra Nov.* 5, 249–257. <https://doi.org/10.1111/j.1365-3121.1993.tb00256.x>
- Roveri, M., Flecker, R., Krijgsman, W., Lofi, J., Lugli, S., Manzi, V., Sierro, F.J., Bertini, A., Camerlenghi, A., De Lange, G., Govers, R., Hilgen, F.J., Hübscher, C., Meijer, P.T., Stoica, M., 2014a. The Messinian Salinity Crisis: Past and future of a great challenge for marine sciences. *Mar. Geol.* 352, 25–58. <https://doi.org/10.1016/j.margeo.2014.02.002>
- Roveri, M., Lugli, S., Manzi, V., Gennari, R., Schreiber, B.C., 2014b. High-resolution strontium isotope stratigraphy of the messinian deep mediterranean basins: Implications for marginal to central basins correlation. *Mar. Geol.* 349, 113–125. <https://doi.org/10.1016/j.margeo.2014.01.002>

- Ryan, W.B.F., 2008. Modeling the magnitude and timing of evaporative drawdown during the Messinian salinity crisis. *Stratigraphy* 5, 227–243.
- Sabino, M., Pierre, F. Dela, Natalicchio, M., Birgel, D., Gier, S., Peckmann, J., 2020. The response of water column and sedimentary environments to the advent of the Messinian salinity crisis : insights from an onshore deep- water section ( Govone , NW Italy ).
- Schildgen, T.F., Cosentino, D., Frijia, G., Castorina, F., Dudas, F.O., Iadanza, A., Sampalmieri, G., Cipollari, P., Caruso, A., Bowring, S.A., Strecker, M.R., 2014. Sea level and climate forcing of the Sr isotope composition of late Miocene Mediterranean marine basins. *Geochemistry, Geophys. Geosystems* 2964–2983. <https://doi.org/10.1002/2014GC005332>.Received
- Schlager, W., 2005. Carbonate Sedimentology and Sequence Stratigraphy. SEPM concepts in sedimentology and paleontology, volume 8, Tulsa, Oklahoma. <https://doi.org/10.2110/csp.05.08>
- Spatola, D., del Moral-Erencia, J.D., Micallef, A., Camerlenghi, A., Garcia-Castellanos, D., Gupta, S., Bohorquez, P., Gutscher, M.-A., Bertoni, C., 2020. A single-stage megaflood at the termination of the Messinian salinity crisis: Geophysical and modelling evidence from the eastern Mediterranean Basin. *Mar. Geol.* 430, 106337. <https://doi.org/10.1016/j.margeo.2020.106337>
- Sprovieri, M., Bonanno, A., Barbieri, M., Bellanca, A., Neri, R., Patti, B., Mazzola, S., 2004.  $^{87}\text{Sr}/^{86}\text{Sr}$  variation in Tortonian Mediterranean sediments: a record of Milankovitch cyclicity, in: D'argenio, B., Fisher, A.G., Premoli Silva, I., Weissert, H., Ferreri, V. (Eds.), *Cyclostratigraphy: Approaches and Case Histories*. Society for Sedimentary Geology 81, pp. 17–26. <https://doi.org/10.2110/pec.04.81.0017>
- Williams, S., Halfar, J., Zack, T., Hetzinger, S., Blicher, M., Juul-Pedersen, T., 2018. Comparison of climate signals obtained from encrusting and free-living rhodolith coralline algae. *Chem. Geol.* 476, 418–428. <https://doi.org/10.1016/j.chemgeo.2017.11.038>
- Yellin-Dror, A., Grasso, M., Ben-Avraham, Z., Tibor, G., 1997. The subsidence history of the northern Hyblean plateau margin, southeastern Sicily. *Tectonophysics* 282, 277–289. [https://doi.org/10.1016/S0040-1951\(97\)00228-X](https://doi.org/10.1016/S0040-1951(97)00228-X)

## Supplementary figures

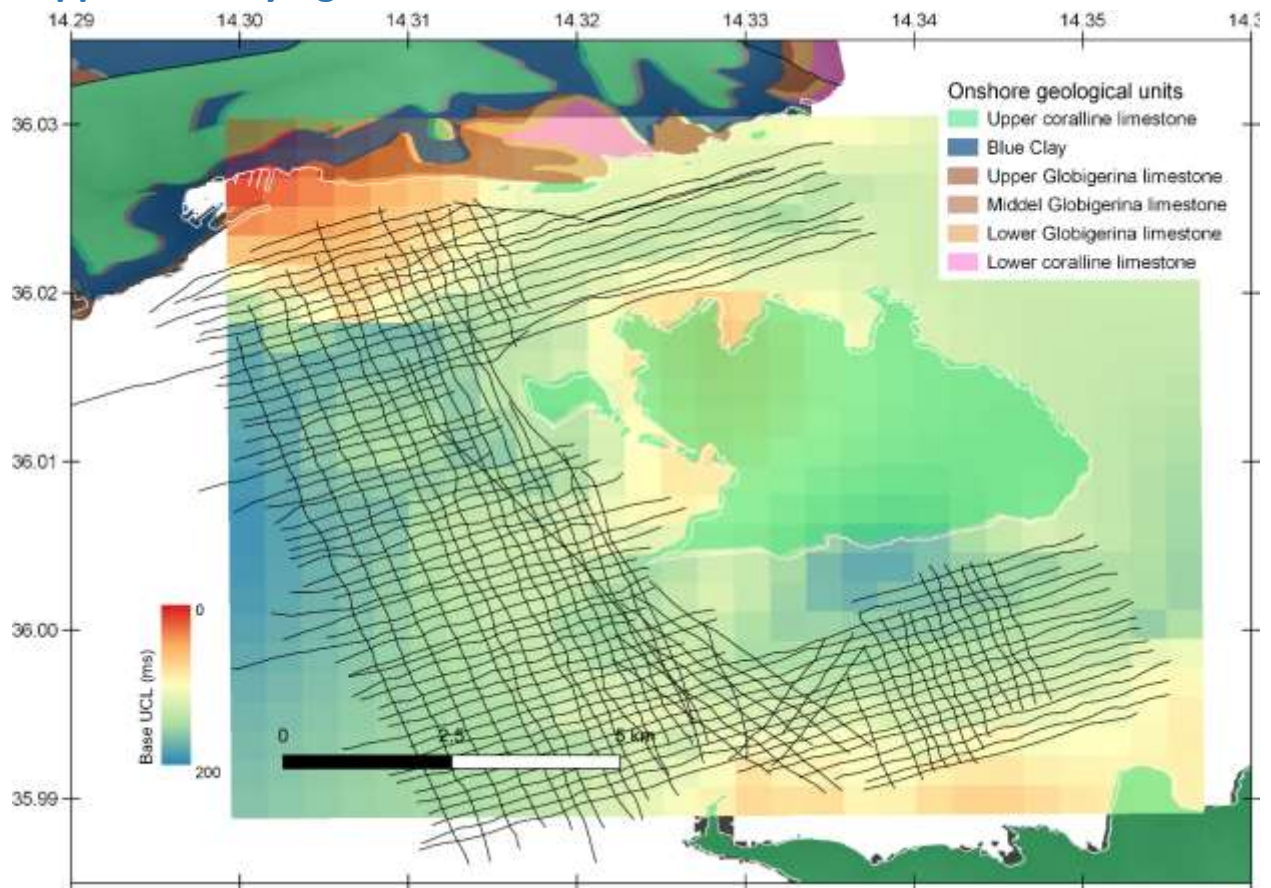


**Figure S1:** extrapolated depth in ms of the base of the UCL.

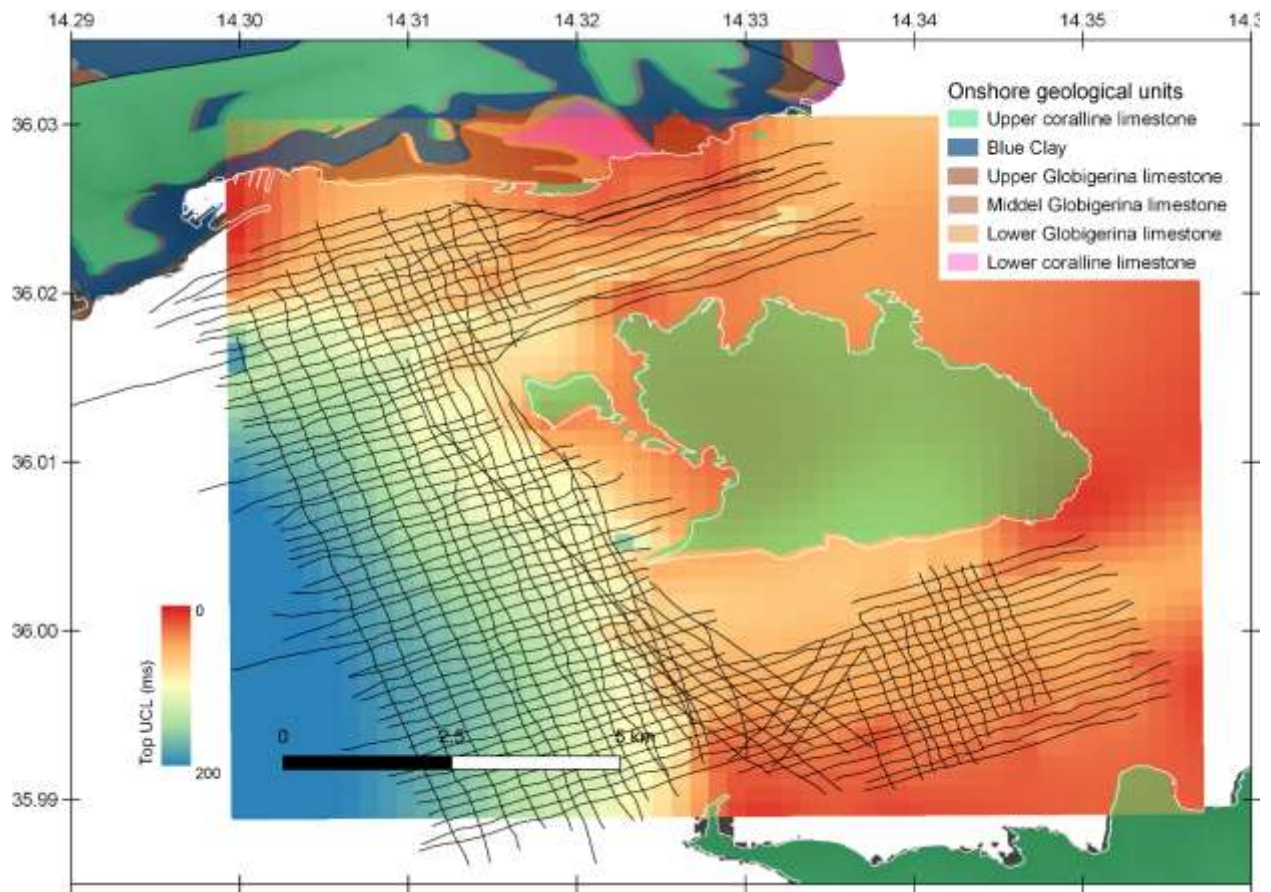


**Figure S2:** extrapolated depth in ms of the top of the UCL.

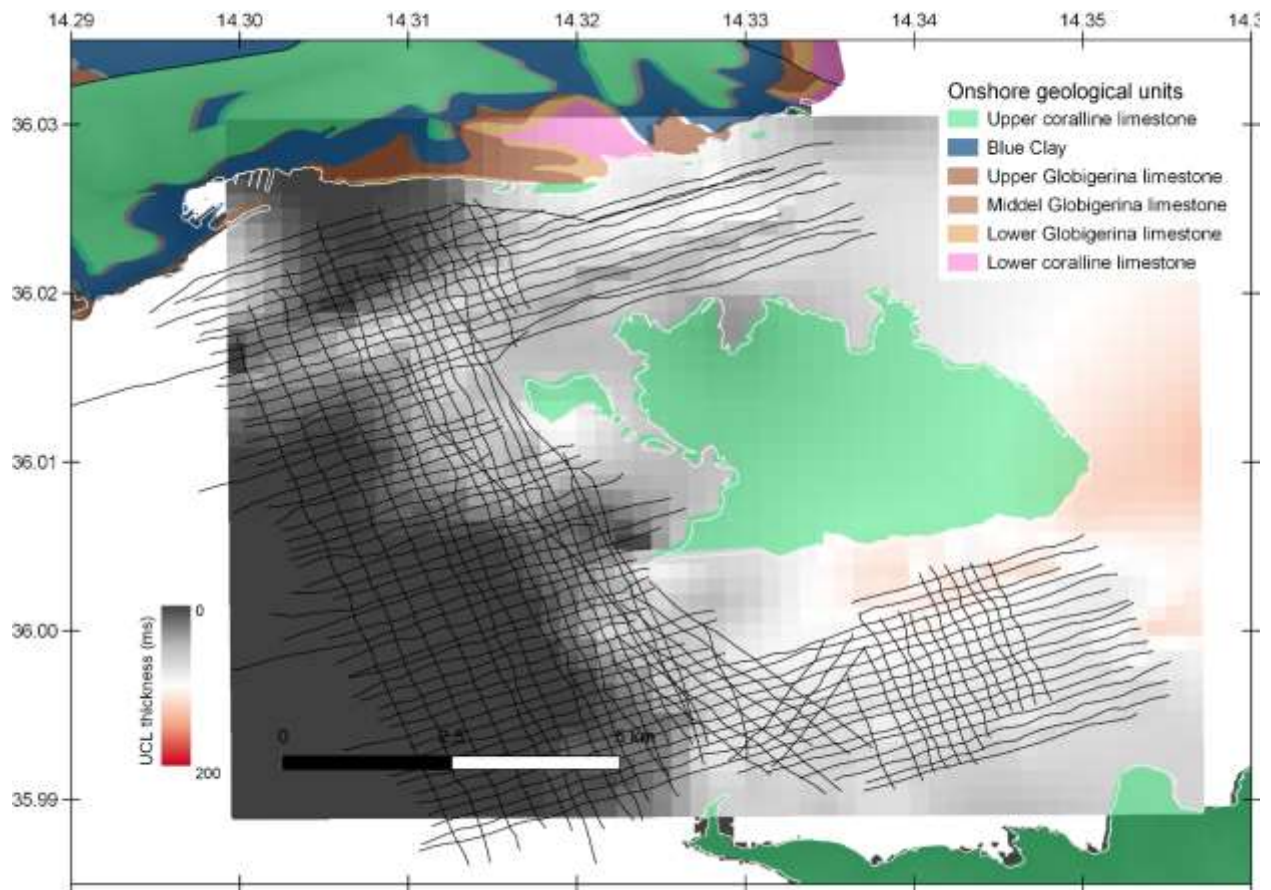


**Figure S3:** extrapolated thickness in ms of the UCL.